World Academy of Science, Engineering and Technology
International Journal of Mechanical and Mechatronics Engineering
Vol:11, No:3, 2017

High-Speed Particle Image Velocimetry of the Flow around a Moving Train Model with Boundary Layer Control Elements

Alexander Buhr, Klaus Ehrenfried

***Abstract*—**Trackside induced airflow velocities, also known as slipstream velocities, are an important criterion for the design of high-speed trains. The maximum permitted values are given by the Technical Specifications for Interoperability (TSI) and have to be checked in the approval process. For train manufactures it is of great interest to know in advance, how new train geometries would perform in TSI tests. The Reynolds number in moving model experiments is lower compared to full-scale. Especially the limited model length leads to a thinner boundary layer at the rear end. The hypothesis is that the boundary layer rolls up to characteristic flow structures in the train wake, in which the maximum flow velocities can be observed. The idea is to enlarge the boundary layer using roughness elements at the train model head so that the ratio between the boundary layer thickness and the car width at the rear end is comparable to a full-scale train. This may lead to similar flow structures in the wake and better prediction accuracy for TSI tests. In this case, the design of the roughness elements is limited by the moving model rig. Small rectangular roughness shapes are used to get a sufficient effect on the boundary layer, while the elements are robust enough to withstand the high accelerating and decelerating forces during the test runs. For this investigation, High-Speed Particle Image Velocimetry (HS-PIV) measurements on an ICE3 train model have been realized in the moving model rig of the DLR in Göttingen, the so called tunnel simulation facility Göttingen (TSG). The flow velocities within the boundary layer are analysed in a plain parallel to the ground. The height of the plane corresponds to a test position in the EN standard (TSI). Three different shapes of roughness elements are tested. The boundary layer thickness and displacement thickness as well as the momentum thickness and the form factor are calculated along the train model. Conditional sampling is used to analyse the size and dynamics of the flow structures at the time of maximum velocity in the train wake behind the train. As expected, larger roughness elements increase the boundary layer thickness and lead to larger flow velocities in the boundary layer and in the wake flow structures. The boundary layer thickness, displacement thickness and momentum thickness are increased by using larger roughness especially when applied in the height close to the measuring plane. The roughness elements also cause high fluctuations in the form factors of the boundary layer. Behind the roughness elements, the form factors rapidly are approaching toward constant values. This indicates that the boundary layer, while growing slowly along the second half of the train model, has reached a state of equilibrium.

***Keywords*—**Boundary layer, high-speed PIV, ICE3, moving train model, roughness elements.

Alexander Buhr is with the German Aerospace Center (DLR)/ Institute of Aerodynamics and Flow Technology/Department Fluid Systems, Göttingen, 37073 Germany (phone: +49-551-709-2521, e-mail: alexander.buhr@dlr.de).

Klaus Ehrenfried is with DLR/Institute of Aerodynamics and Flow Technology/Department Fluid Systems, Göttingen, 37073 Germany (e-mail: klaus.ehrenfried@dlr.de).

I. Introduction

THE aerodynamic design of high-speed trains is optimized for fast travelling at low energy consumption and crosswind stability. An equally important design criterion are the flow velocities induced to the surroundings. High air speed constitutes a potential risk for nearby workers and objects. Therefore, the maximum induced flow velocities at specific positions next to the track are limited by a European standard, the Technical Specifications for Interoperability (TSI, [1]). For train manufactures it is of great interest to know in advance, how new train geometries would perform in admission tests. Previous studies have shown, that the maximum flow velocities for different high-speed train geometries occur in the near wake (cf. [2]). It is assumed, that maximum velocities are caused by the flow structures in the near wake, which develop from the flow around the rear end of the train. The boundary layer rolls up to specific vortex formations (cf. [3]). Depending on the end car shape, the rear end flow is dominated by an asymmetrical separation of vertical vortices combined with a mixing overflow.

A common method for flow investigations are model experiments. Since one of the TSI specific measurement positions is low above the top of rail, the relative movement between model and ground is assumed to be an important issue. The tunnel simulation facility Göttingen (TSG, see Section III-A) is a moving model rig, which provides realistic train speeds and allows transient measurements at various ground conditions. Nevertheless, most moving model rigs are limited to the model size and in particular the model length. As a result, the Reynolds number is multiple times lower depending on the scale factors compared to full-scale. As mentioned above, it is assumed, that the boundary layer condition at the rear end determines the wake flow structure and therefore the maximum flow velocities. The idea is to control the boundary layer thickness by widening and to create a flow around the rear end, which is more comparable to full-scale trains. Therefore, vortex generators or so called roughness elements can be mounted in the train head section to widen the boundary layer. In this study, the main objective is to compare the effect of different head roughnesses with a clean head shape in view of the boundary layer development. Therefore, three roughness element designs are tested to compare the influence of roughness characteristics at different model heights. A model train with a simplified ICE3 geometry is tested (see Section III-C), which allows a full-scale comparison in further investigations. High-Speed

Particle Image Velocimetry (HS-PIV, see Section III-B) is an improved, non-intrusive measurement system, which is used for two-dimensional velocity measurements close to the model wall with a sufficient spacial and temporal resolution.

II. Boundary Layer Control

In this investigation, a special boundary layer control method is tested to simulate a longer train model and a thicker boundary layer at the rear end according to a higher Reynolds number. For further informations about the influence of the train length on the wake flow see [4]. Fig. 1 illustrates, how roughness elements are used as vortex generators to widen the boundary layer and create a specific thickness δ respective to a longer train. This method has already been used in wind tunnel experiments for slipstream investigations (cf. [5]).

As mentioned in Section I, the lower Reynolds number in moving model rigs results in a different flow around the train geometry compared to full-scale. Previous studies have shown, that the flow structures in the near wake usually yield the maximum velocities at the specific measurement position for TSI validation tests (cf. [2]). The hypothesis is, that the flow around the end car has a major effect on the development of the wake flow structures. The idea is to control the boundary layer with vortex generators at the model head to create a more realistic ratio between boundary layer thickness and model width without introducing artificial flow structures at the rear end. As shown in Fig. 1, the vortex generators widen the boundary layer at the first car of the short train (blue). By the use of a specific roughness configuration, both models reach a similar boundary layer thickness δ at the rear end. It is expected, that the boundary layer profile is completely disturbed by the roughness along the first and middle car, but stabilize after a specific model length.

For the boundary layer control investigation, the first car is replaced with a generic dummy car, which is formed with the use of superellipses to avoid flow separation. The second half of the first car can be equipped with vortex generators. Therefore, so called roughness elements are used, which add small rectangle obstacles with specific sizes and order to the surface. Due to the braking concept and the high mechanical load during deceleration, the roughness elements have to be small and robust. For the optimal shape, small roughnesses are used, which size have a relative high equivalent sand roughness according to Nikuradse [7]. It is assumed, that rectangular vortex generators are the best choice to gain a sufficient impulse loss at a short length. Further informations about the comparison between different obstacle shapes and equivalent sand roughnesses can be found in [8]. To avoid artificial flow structures inside the boundary layer, every second roughness element is vertical mirrored. Hereby, small vortices created at the edge of a vortex generators are eliminated by the next element. A more detailed description of the roughness elements can be found in Section III-C.

III. Experimental Setup

A. Tunnel Simulation Facility Göttingen

The tunnel simulation facility Göttingen (TSG) is a moving model rig for aerodynamic and aeroacoustic measurements

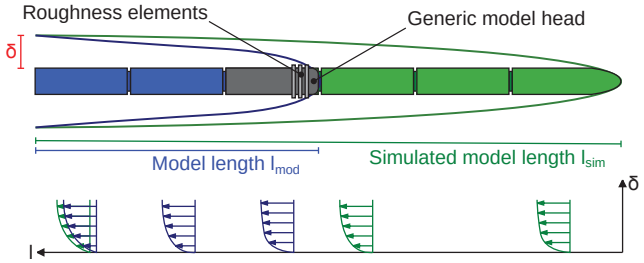

Fig. 1 Boundary layer control with roughness elements in the head section of a short train model l_{mod} for simulating a larger model length l_{sim} (cf. [6])

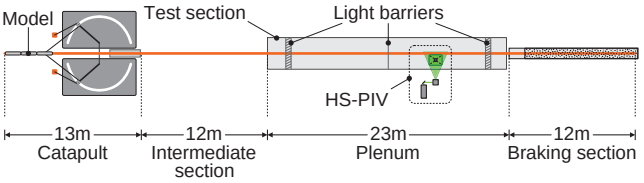

Fig. 2 Overview of the tunnel simulation facility Göttingen (cf. [6])

on train models. Fig. 2 gives a short overview of the four functional sections: catapult, intermediate section, plenum and braking section. A detailed technical description and further applications can be found in [6].

Compared to conventional wind tunnel facilities, the TSG allows transient measurements with moving train models passing the test section. Furthermore, the TSG provides a correct relative movement between model and ground, which is assumed to be essential for a realistic development of the boundary layer and wake flow. The TSG is designed for train models scaled 1:25 with a maximum length of $2.5\,\mathrm{m}$ to $3\,\mathrm{m}$, which corresponds to approximately three coaches. The model scale and especially the decreased model length result in a significant difference in the Reynolds number compared to full-scale trains. As mentioned in Section II, the boundary layer control of the train model is an attempt to simulate an increased model length and to create a more comparable boundary layer profile at the rear end. The ground conditions in the test section can be setup to different track geometries like flat ground or STBR (single track ballast and rail). The model speed and position during a test run are determined by 5 light barriers within the test section. Various measurement systems like surface pressure probes, Pitot rakes, hot-wire probes or (High-Speed) Particle Image Velocimetry (see Section III-B) can be installed. According to the complexity of the measurement system, it takes $10\,\mathrm{min}$ to $30\,\mathrm{min}$ between two launches. The ambient conditions can be reproduced very good and the variation of the model speed is less than $0.15\,\mathrm{m/s}$ from run to run.

B. High-Speed Particle Image Velocimetry

Particle Image Velocimetry (PIV) is an optical, non-intrusive measurement method for flow velocities within a defined spatial plane. The flow velocity is determined by the displacement of tracer particles, which are laser-illuminated and recorded by a camera. A detailed description of the PIV-technique can be found in [9]. For this investigation, a transient flow with high velocities and dynamics is expected.

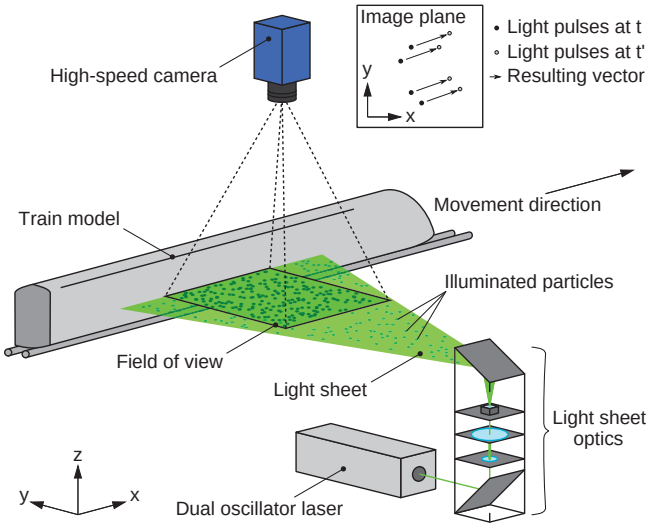

Fig. 3 Overview of the flow velocity measurement using High-Speed Particle Image Velocimetry at the tunnel simulation facility Göttingen (cf. [11])

Therefore, High-Speed PIV (HS-PIV) is used to achieve a proper spatial and temporal resolution. A dual oscillator pulsed laser with an arbitrary low separation time combined with an high-speed camera allow a sampling rate $\geq 1\,\mathrm{kHz}$.

Fig. 3 gives a short overview of the HS-PIV setup at the TSG used in this investigation. The light sheet plane is created by a Quantronix Darwin Duo dual oscillator laser combined with special light sheet optics set in the light path. This laser produces two pulses at t and $t' = t + \Delta t$ with a specific separation time Δt. The separation time Δt determines the temporal resolution and is adjusted to the assumed flow velocities and dynamics. The light sheet is orientated parallel to the ground and perpendicular to the track. The entire plenum is seeded with DEHS (di-ethyl-hexyl-sebacat) tracer particles to ensure a homogeneous seeding with a sufficient density. A pco.dimax high speed camera with a 1.4/85 mm Zeiss lens is mounted $1.4\,\mathrm{m}$ above the flat ground to record an image of the illuminated tracer particles every t and t'. The flow velocity is determined using cross-correlation of every image pair (t,t') (*frame-straddling*, see [9]). The PIVview software is used for data post-processing and cross-correlation of the recorded double-images (see [10]).

HS-PIV yields informations about the velocity magnitude $v_{\mathrm{flow}} = |\vec{v}_{\mathrm{flow}}|$ and the velocity components $v_{\mathrm{x,flow}}$, $v_{\mathrm{y,flow}}$. This allows an analysis of the boundary layer and the flow structures. The spatial resolution depends on the camera position and chip resolution as well as the seeding density. The separation time and the sampling rate of laser and camera define the temporal resolution. A more detailed description of a similar HS-PIV measurement can be found in [6].

C. ICE3 Train Model

In this investigation, a three-parted train model with a 1:25 scaled ICE3 middle and end car is used. The first car has a generic geometry formed with superellipses to avoid separation and provide approximately a potential flow around the model head. The overall length of the train model is $2.27\,\mathrm{m}$. The second half of the first car is designed modifiable. Vortex generators or so called roughness elements can be attached at four positions. Every second element is vertical mirrored to eliminate artificial induced streamwise vortices at the roughness edges. The model cars are separated through small gaps at $x_{\mathrm{gap1}} = 0.5\,\mathrm{m}$ and $x_{\mathrm{gap2}} = 1.225\,\mathrm{m}$, which represent the inter-car gaps at full-scale trains. One additional gap separates the model head from the modifiable second half. The rear end of the ICE3 is streamlined compared to previous investigated geometries like a double-deck train [11]. Multiple bogies and bumpers are installed at the underbody.

Fig. 4 ICE3 train model scaled 1:25 with four head configurations (CLEAN, RGH-1, RGH-2, RGH-3) using three different roughness element designs

The train model can be set up to four configurations with three different roughness conditions (RGH-1,2,3) as shown in Fig. 4. The three elements differ in the roughness size at the side and top area as well as the shape of the lowest roughness edge:

CLEAN: No roughness elements,
no inter-car gaps at first car

RGH-1: Roughness elements (white), inter-car gaps,
↪ 6 mm side, 7 mm top, lowest edge small

RGH-2: Roughness elements (red), inter-car gaps
↪ 6 mm side, 10 mm top, lowest edge large

RGH-3: Roughness elements (green), inter-car gaps
↪ 9 mm side, 11 mm top, lowest edge large

The measured side of the train model is painted black at the height of the light sheet plane, because of interfering light reflections through the HS-PIV setup.

D. Measurements

The boundary layer study on the ICE3 train model (see Section III-C) were performed at the tunnel simulation facility Göttingen (TSG, see Section III-A) using High-Speed Particle Image Velocimetry (HS-PIV, see Section III-B). A flat ground condition is used to investigate the basic effect of different head roughness conditions. The light sheet plane of the HS-PIV is set up to 8 mm above top of rail (TOR), which is 6.8 mm above the flat ground. As shown in Fig. 2, the

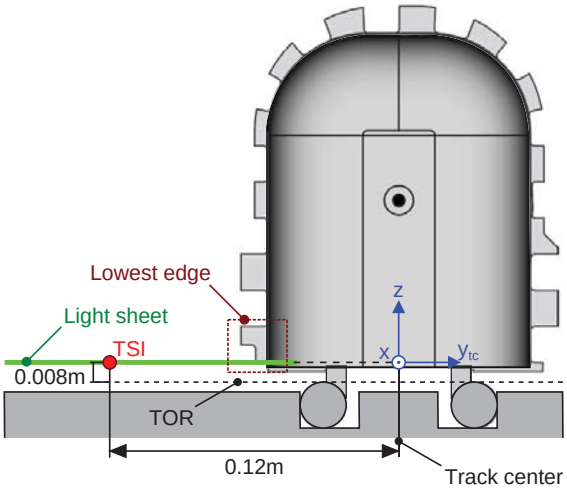

Fig. 5 Profile view of the TSG test section with an ICE3 train model and HS-PIV. The light sheet is set up to a height of 8 mm above top of rail (TOR) and contains the scaled TSI measurement position at a distance of 0.12 m from the track center

HS-PIV setup is located in the second half of the test section between the middle and last light barriers.

Fig. 5 shows a profile view of the ICE3 train model with the RGH-1 head configuration. The scaled TSI measurement position is located 0.008 m above the top of rail (TOR8) at a distance of $y_{tc} = 0.12\,\mathrm{m}$. The light sheet height corresponds to the underbody region of the train model. Due to the curve of the model surface, the camera view on the light sheet close to the model surface is obscured. It is estimated, that the gap from the visible region to the model surface is smaller than 3 mm. In this setup, the measurement section is about $0.271\,\mathrm{m} \times 0.177\,\mathrm{m}$, which corresponds to an image resolution of $1916\,\mathrm{px} \times 1248\,\mathrm{px}$. The orientation of the measurement area is shown in Fig. 5. x corresponds to the movement direction of the train model. y_{tc} corresponds to the distance from the track center (tc). The image pairs are recorded with a separation time $\tau = 80\,\mu\mathrm{s}$ and a sampling rate of 1 kHz in frame-straddling mode (cf. [9]). The TSG catapult pressure is adjusted to a model speed of $u_{mod} = 32\,\mathrm{m/s}$. The actual model speed varies about $\pm 0.15\,\mathrm{m/s}$. A pre-trigger of 1 s is set to record the head wave effect. The internal camera memory provides a recording time of about 5 s. According to this setup, the train model passes the measurement area in 0.079 s or 79 double-images. Previous measurements have shown, that a number of 30 test runs per configuration provides sufficient statistics with a decent expenditure of time. This results in overall 120 test runs for the four configurations.

IV. Results

A. Flow Velocity Measurement

The test runs were performed using HS-PIV as described in Section III-D. Fig. 6 illustrates the measurement area seen by the camera with the used grid points, on which the flow velocity is analysed. The PIV analysis parameters are adjusted to the expected flow velocities and dynamics. The interrogation window size is set to 32 px with a step size of 16 px. This

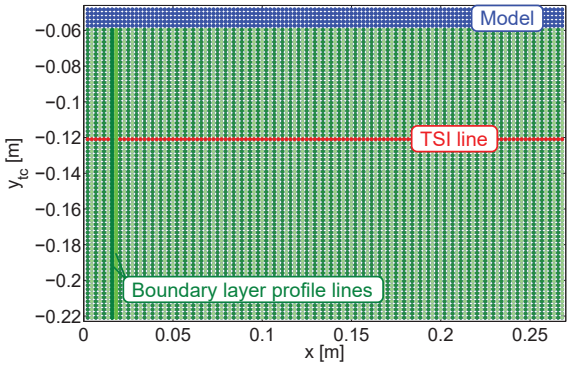

Fig. 6 Illustration of the measurement area with the analysed grid positions (green). The model passes the recorded images at the upper edge from left to right. The model area (blue) is masked out and the TSI related distance is marked red

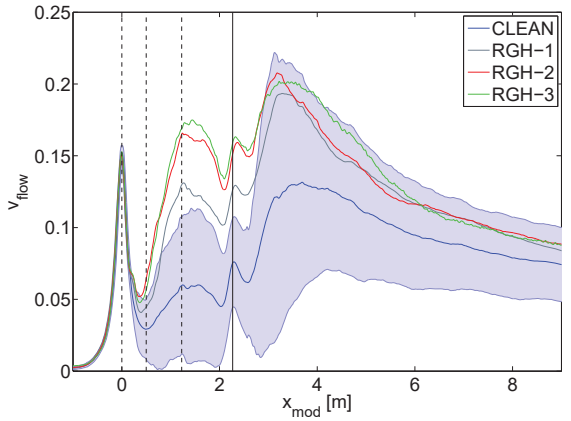

Fig. 7 Normalized flow velocities v_{flow} averaged over the TSI line for all configurations in comparison. Additionally, the standard deviation $\sigma_{v_{flow}}$ is exemplary plotted for the clean configuration (blue area)

results in 118 grid points at a consistent distance y_{tc} from the track and $118 \times 77 = 9086$ grid points overall. The train model passes the images within the blue area from left to right, which is masked out in the analysis. The model wall is located at around $y_{tc} = -0.06\,\mathrm{m}$. The TSI related lateral distance of $y_{tc} = -0.12\,\mathrm{m}$ is marked red. The light green and dark green dots show the measurement positions considered in the boundary layer analysis in Section IV-C. The separated vertical lines in light and dark green show the analysed grid lines for boundary layer profiles at specific x_{mod}.

The measured flow velocities are normalized with the model speed u_{mod} for every single run to get a better comparability between runs and configurations. It should be noted, that these are transient measurements and show a passing of the train model. The time-dependent data $v_{flow}(t)$ is resampled to location-dependent data $v_{flow}(x)$ using the model speed and specific model position information from the image sequence. In this way, the data can be transformed into the model coordinate system x_{mod}. A detailed description of the resampling method can be seen in [6]. Thereby, the flow velocities $v$flow for every distance y_{tc} can be averaged along the model x_{mod}.

Fig. 7 shows the averaged, normalized flow velocities v_{flow} at $y_{tc} = -0.12\,\mathrm{m}$ for all configurations in comparison.

Additionally, the standard deviation $\sigma_{v_{\text{flow}}}$ for the clean configuration is marked as a blue area to show exemplary the high fluctuation of the unsteady flow between the single runs. The first dotted line marks the train nose at $x_{mod} = 0\,\text{m}$. The second and third dotted line mark the inter-car gaps and the solid line marks the rear end of the train model at $x_{\text{mod}} = 2.27\,\text{m}$. As expected, the head wave is very similar in all configurations. The good reproducibility is ascribed to the potential flow around the generic model head. It should be noted, that the head wave is artificially increased, due to high displacement of the generic head shape.

The differences between the three roughness element designs are described in Section III-D. It is assumed that the lowest roughness edge has a major influence on the measured velocities, because it is located at the same height (see Fig. 5). As mentioned, the lowest roughness edge is significantly smaller for RGH-1 compared to RGH-2 and RGH-3, while the lowest roughness edge of RGH-2 and RGH-3 is identical (see Fig. 4). Behind the head wave $x_{\text{mod}} > 0.5\,\text{m}$, the flow velocities for RGH-1,2,3 are significantly increased by the roughness elements compared to the CLEAN configuration. RGH-2 and RGH-3 show a similar increase, while the increase for RGH-1 is smaller. The roughnesses for RGH-3 are larger at the side and top level compared to RGH-2, but the flow velocities show just a small increase between RGH-2 and RGH-3. This matches with the assumed major effect of the lowest roughness edge.

In the near wake behind the model, the flow velocities for RGH-1, RGH-2 and RGH-3 are increased compared to the CLEAN configuration as well. Here, RGH-3 shows an additional widening of the maximum peak compared to RGH-2. This is ascribed to the larger roughness in the top region. A first hypothesis is, that the size of the roughness edges effect the flow on their specific height along the train model. A larger roughness in the lowest position influences the direct wave beside the model, due to the least distance to the measuring position. A larger roughness in the upper height causes a stronger overflow at the rear end, which falls downwards behind the model and merges with the direct wave at farther x_{mod}. In the following, the investigation concentrates on the flow by the side of the train model, especially the boundary layer velocities and parameters. The effect of the boundary layer control on the wake flow will be part of further investigations.

B. Boundary Layer Visualization

The resampled flow velocity data $v_{\text{flow}}(x)$ is used to visualize the average boundary layer along the train model for a qualitative comparison. Therefore, the flow velocities at every model position x_{mod} are averaged over the 118 boundary layer profile lines shown in Fig. 6. Noting potential redundant informations due to the small distance between the boundary layer profiles, this averaging provides significant better statistics.

Fig. 8 shows the resulting flow velocities v_{flow} of the boundary layer profiles along the train model x_{mod} for all configurations in comparison. The magnitude of the flow velocity within the x-y-plane is indicated by the color from $v_{\text{flow}} = 0$ deep blue to $v_{\text{flow}} = 0.8$ deep red. Additionally, the TSI related distance to the model is marked with a dashed red line at $y_{\text{tc}} = -0.12\,\text{m}$. The head wave near $x_{\text{mod}} = 0\,\text{m}$ is very similar in each configuration, as suggested by the averaged flow velocities in Fig. 7. Behind the head wave, the flow velocity decreases to nearly $v_{\text{flow}} = 0$, which can be related to a reverse flow also observed in previous studies. At about $x_{\text{mod}} = 0.1\,\text{m}$ the flow velocity increases in all configurations. The area of the maximum velocities is located near the middle of the first car for the CLEAN configuration and in the second third of the first car for the RGH-1,2,3 configurations. The increased velocities are ascribed to the bogie on the underbody. The bogie acts like an additional roughness, which can be seen in the CLEAN configuration. In case of RGH-1,2,3, the roughness elements significantly increase the flow velocities near the model surface and expand the increased velocity area to the second third, due to their mounting positions. The maximum magnitude of the flow velocity reach 0.5 for the CLEAN, 0.6 for the RGH-1 and 0.8 for the RGH-2 and RGH-3 configurations. The near-wall maximum flow velocities show a significant decrease behind the first car for all configurations, but the resulting area effected by the model is still increased in y-direction. The overall flow velocities along the end car are increased for RGH-1 compared to CLEAN.In case of RGH-2 and RGH-3 the flow velocities are even more increased compared to RGH-1, but show a quite similar development characteristic. At $x_{\text{mod}} = 2\,\text{m}$ all configurations show a small decrease, which can be referred to the flow around the model end shape. It is assumed, that this flow develops into the near wake and effects the wake flow structures.

Fig. 9 shows the flow velocity fluctuations $\sigma_{v_{\text{flow}}}$ along the train model x_{mod} analogous to Fig. 8. As mentioned in Section IV-A, the measured velocities vary greatly between the single runs. Also, the flow velocities of the boundary layer profiles within the measurement area vary, due to the high turbulent, transient flow. In the head wave area, the fluctuations are very low and only located close to the surface for all configurations. As already seen in Fig. 7, the fluctuations in the head wave are nearly zero at the TSI related distance $y_{\text{tc}} = -0.12\,\text{m}$. In case of the CLEAN configuration, the influence of the bogie

As expected, the roughness elements induce high turbulences nearby compared to the CLEAN configuration. Nevertheless, the fluctuations show a very similar behaviour compared to the velocity magnitude. Along the end car, the range of influence perpendicular to the model wall is increased for RGH-1,2,3 compared to CLEAN. It is also notable, that in case of the rough configurations RGH-1,2,3 a higher magnitude of velocity as well as velocity fluctuations reaches the TSI related distance $y_{\text{tc}} = -0.12\,\text{m}$ significantly earlier compared to the CLEAN configuration.

These qualitative observations correspond very well to the average flow velocity shown in Fig. 7. To get more quantitative results for the boundary layer, typical parameters are calculated in Section IV-C to characterize each boundary layer development for every configuration.

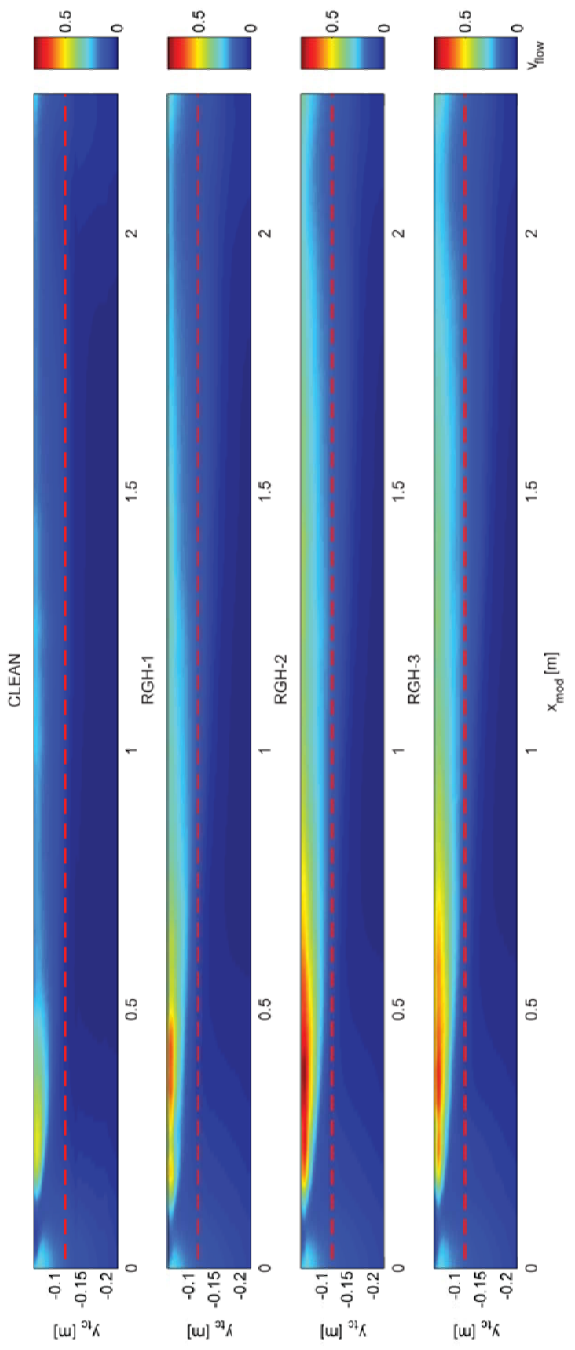

Fig. 8 Visualization of the boundary layer for the four configurations with averaged, normalized flow velocities v_{flow} along the ICE3 model x_{mod}

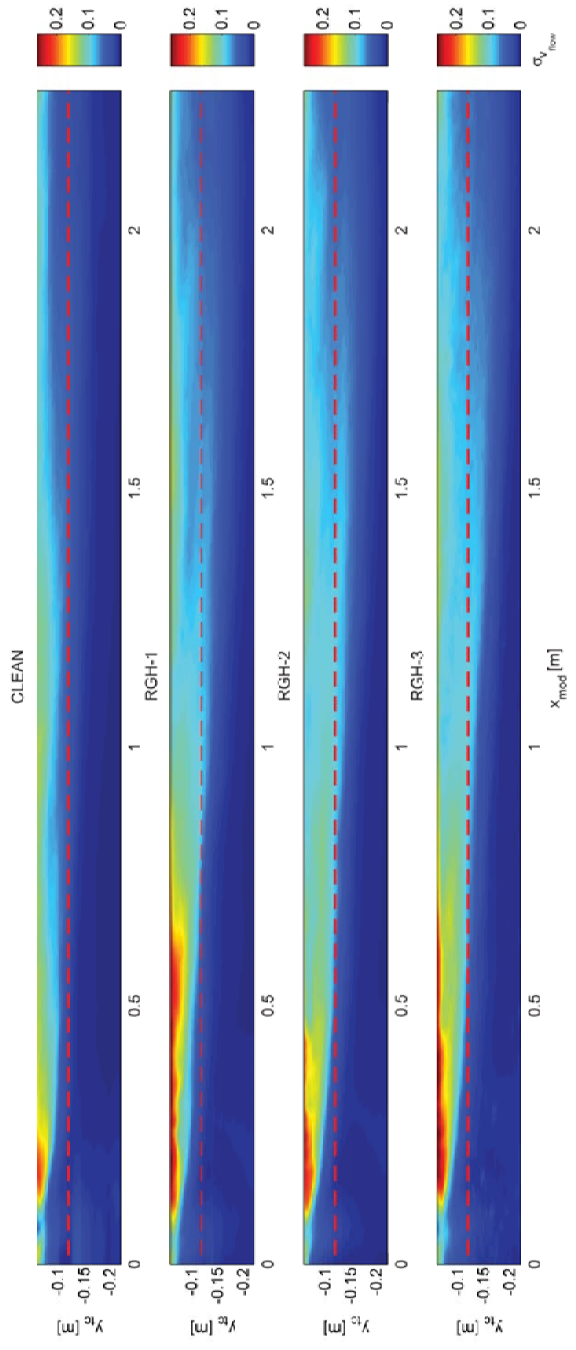

Fig. 9 Visualization of the averaged velocity fluctuations $\sigma_{v_{\text{flow}}}$ for the four configurations along the ICE3 model x_{mod}

C. Boundary Layer Study

In the following study, boundary layer parameters like boundary layer thickness δ_{99}, displacement thickness δ_1, momentum thickness δ_2 and form factor H_{12} are calculated. These quantitative results are used to confirm the previous qualitative observations. For these calculations, only the x-component of the flow velocities $v_{\text{x,flow}}$ is relevant. The integral calculation methods for δ_1 and δ_2 require normalized velocities, which are already determined. Thereby, the flow velocities $v_{\text{x,flow}}$ measured in the stationary frame of reference can be transformed to the model frame of reference $v^{\text{mod}}_{\text{x,flow}}$ as follows:

$$v^{\text{mod}}_{\text{x,flow}} = 1 - v_{\text{x,flow}} \tag{1}$$

Fig. 10 shows exemplary the normalized, averaged boundary layer profiles at $x_{\text{mod}} = 2\,\text{m}$ of all configuration in comparison. The normalized, averaged velocities $v_{\text{x,flow}}$ in these profiles are used to calculate δ_{99}, δ_1, δ_2 and H_{12} for each x_{mod} along the train model. At this near-end model location, the boundary layer profiles look very similar, only increased in

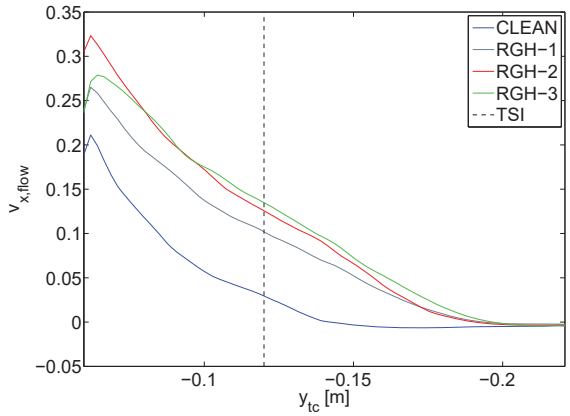

Fig. 10 Boundary layer flow velocities $v_{\mathrm{x,flow}}$ in a profile view perpendicular to the model wall $y_{\mathrm{tc}} = -0.06\,\mathrm{m}$ at the rear end $x_{\mathrm{mod}} = 2.2\,\mathrm{m}$ for all configurations in comparison

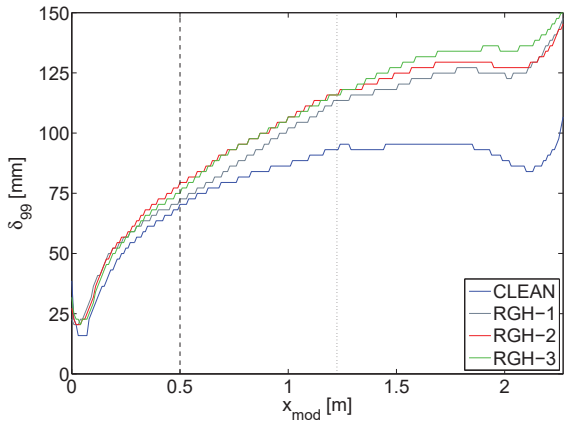

Fig. 11 Boundary layer thickness δ_{99} along the train model x_{mod} for all configurations in comparison (gap1 dashed line, gap2 dotted line)

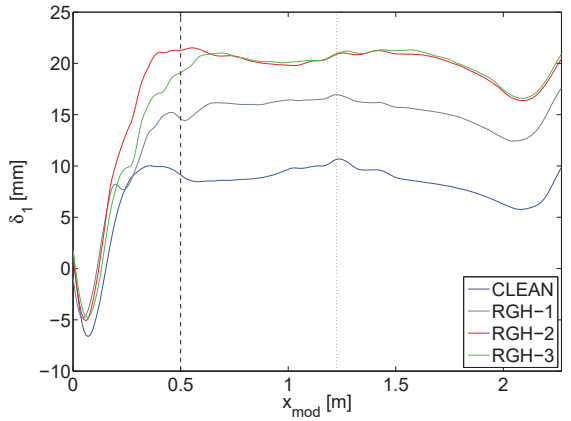

Fig. 12 Displacement thickness δ_1 along the train model x_{mod} for all configurations in comparison (gap1 dashed line, gap2 dotted line)

the magnitude for the rough configurations RGH-1,2,3. As seen in Fig. 7 and in the boundary layer visualization (see Fig. 8), the velocity increase for RGH-2 and RGH-3 is larger compared to RGH-1. It is assumed, that this can be ascribed to the larger near-ground roughness edge for RGH-2 and RGH-3 (cf. Fig. 4). RGH-2 and RGH-3 show a similar boundary layer profile at this measurement height, even though the roughness is different at upper model heights. This approves the hypothesis, that the roughness elements mainly effect the boundary layer at the respective height along the train model.

1) Boundary Layer Thickness: The boundary layer thickness δ_{99} is defined as the distance to the wall at which the flow velocity reaches 99% of the inflow. Considering (1), in moving model measurements, δ_{99} is defined analogous as the distance to the model wall at which the measured flow velocity decreases to 1% of the model speed u_{mod} or 0.01 as a normalized value. It is also common, that δ_{99} is very hard to define due to the measurement inaccuracy. Fig. 11 shows the development of δ_{99} along the train model x_{mod} for all configurations in comparison. δ_{99} is determined by the first grid position in y_{tc} measuring a flow velocity $v_{\mathrm{x,flow}} < 0.01$. This determination method leads to discrete values, due to the spatial resolution of the analysed PIV grid (see Fig. 6). The comparison of δ_{99} already indicates the observations mentioned before. The rough configurations show an increase in δ_{99}, especially along the middle and end car compared to the CLEAN head shape. With this parameter, the rough configurations RGH-1,2,3 show a very similar development of the boundary layer. The values for δ_{99} at $x_{\mathrm{mod}} = 2.2\,\mathrm{m}$ with calculated errors are shown in Table I. The calculation of $\sigma_{\delta_{99}}$ considers the variation of $v_{\mathrm{x,flow}}$ and the resulting inaccuracy of y_{tc} according to the $0.01u_{\mathrm{mod}}$ condition.

2) Displacement Thickness: The displacement thickness δ_1 is calculated analogue to the definition by [8] in the model frame of reference using (1). The flow velocities $v_{\mathrm{x,flow}}$ are normalized with the model speed u_{mod}. This leads to a calculation of δ_1 as follows:

$$\delta_1 = \int_{y_{\mathrm{tc,min}}}^{y_{\mathrm{tc,max}}} v_{\mathrm{x,flow}} dy \qquad (2)$$

Based on the definition and the integral calculation method, δ_1 is more accurate to determine than δ_{99}. The bounds of integration $y_{\mathrm{tc,min}}$ and $y_{\mathrm{tc,max}}$ are given by the size of the analysed measurement area (cf. 6). Fig. 12 shows the resulting values for δ_1 along the train model x_{mod} for all configurations in comparison. It is notable, that the high displacement of the flow around the generic head leads to flow velocities $v_{\mathrm{x,flow}} > u_{\mathrm{mod}}$ in the model frame of reference or a reverse flow $v_{\mathrm{x,flow}} < 0$ in the stationary frame of reference. Combined with the roughness elements, the first car creates an artificial development of the boundary layer and so of the displacement thickness. In this study, the focus is on the middle and end car ($x_{\mathrm{mod}} > 1\,\mathrm{m}$). As excepted, the displacement thickness is increased for the rough configurations RGH-1,2,3. Again, RGH-1 is increased compared to CLEAN and RGH-2,3 are increased compared to RGH-1. The displacement thickness for RGH-2 and RGH-3 is nearly equal. The further development is very similar for all configurations. This confirms the hypothesis, that the roughness elements cause an increase of the boundary layer thickness at the specific height of the roughness edge. The small lowest roughness of RGH-1 causes a smaller increase compared to RGH-2 and RGH-3 with larger lowest roughness. Is is notable, that in case of CLEAN and RGH-1 δ_1 decrease behind the inter-car gap

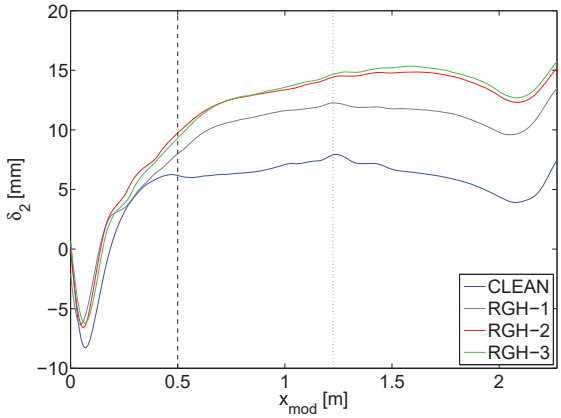

Fig. 13 Momentum thickness δ_2 along the train model x_{mod} for all configurations in comparison (gap1 dashed line, gap2 dotted line)

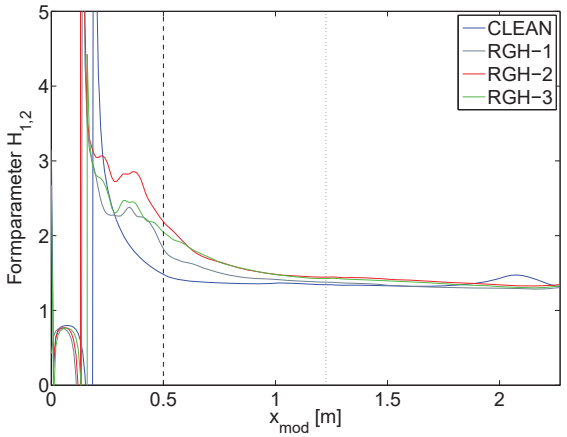

Fig. 14 Form factor H_{12} along the train model x_{mod} for all configurations in comparison (gap1 dashed line, gap2 dotted line)

between the middle and end car (gap2) at $x_{\text{mod}} = 1.225\,\text{m}$ (dotted line). In case of RGH-2 and RGH-3 δ_1 decrease a bit farther behind, but similar to CLEAN and RGH-1. It is assumed, that the inter-car gap and the bogies in this area cause an additional displacement, which lead to this decrease. Further investigations have to be done with focus on this effect. The values for δ_1 at $x_{\text{mod}} = 2.2\,\text{m}$ with calculated errors using error propagation are shown in Table I. Compared to the CLEAN configuration, δ_1 is increased for RGH-1 by 115%, for RGH-2 by 160% and for RGH-3 by 165%. At the rear end an abrupt increase is observed in all configurations, which can be ascribed to the flow around the rear end like an end wave.

3) Momentum Thickness: The momentum thickness δ_2 is calculated analogue to the definition by [8] in the model frame of reference using (1). Due to the definition, the calculation is the same for the stationary and the model frame of reference. The flow velocities $v_{\text{x,flow}}$ are normalized with the model speed u_{mod}. This leads to a calculation of δ_2 as follows:

$$\delta_2 = \int_{y_{\text{tc,min}}}^{y_{\text{tc,max}}} (1 - v_{\text{x,flow}}) \cdot v_{\text{x,flow}} dy \tag{3}$$

As the displacement thickness, the momentum thickness is a more accurate parameter for a boundary layer study. Fig. 13 shows the resulting values for δ_2 along the train model x_{mod} for all configurations in comparison. The observations are almost the same as for the displacement thickness δ_1. It is notable, that the momentum thickness seem to need a longer model length $x_{\text{mod}} > 1.5\,\text{m}$ to reach a specific stable state. As observed in δ_1, δ_2 seems to be affected by the inter-car gap between the middle and end car (gap2) at $x_{\text{mod}} = 1.225\,\text{m}$. The additional displacement might cause a shift in the boundary layer and a loss of momentum. Another reason might be a ground effect, which has to be investigated in further measurements. The values for δ_2 at $x_{\text{mod}} = 2.2\,\text{m}$ with calculated errors using error propagation are shown in Table I. Compared to the CLEAN configuration, δ_2 is increased for RGH-1 by 130%, for RGH-2 by 170% and for RGH-3 by 180%.

4) Form Factor: The form factor H_{12} provides informations about the nature of the flow and can be used to analyse the shape development and stabilization of the boundary layer. The form factor is calculated analogue to the definition by [8] for this measurement as follows:

$$H_{12} = \frac{\delta_1}{\delta_2} \tag{4}$$

Fig. 14 shows the development of H_{12} along the train model x_{mod} for all configurations in comparison. Due to the zeros in δ_1 and δ_2, the form factor shows a not interpretable behaviour in the head area. The assumed stabilization of the boundary layer can be observed from $x_{\text{mod}} > 1\,\text{m}$. The values for H_{12} at $x_{\text{mod}} = 2.2\,\text{m}$ with calculated errors using error propagation are shown in Table I. All configurations reach a quite constant and also similar value around $H_{12} = 1.3$. It is notable, that this value is comparable to a form factor of a turbulent flow around a flat plate of $H_{12} = 1.4$ (cf. [12]). In case of the CLEAN configuration, the form factor shows a small increase near the rear end, which can be ascribed to the small values of δ_1 and δ_2 and the three times larger error.

TABLE I
RESULTS FOR BOUNDARY LAYER PARAMETERS δ_{99}, δ_1, δ_2 AND $H_{1,2}$ NEAR THE MODEL REAR END AT $x_{\text{MOD}} = 2.2\,\text{m}$

	δ_{99} [mm]	δ_1 [mm]	δ_2 [mm]	H_{12}
CLEAN	89 ± 4	6.8 ± 0.9	4.9 ± 0.7	1.4 ± 0.3
RGH-1	136 ± 5	14.6 ± 1.1	11.3 ± 0.8	1.3 ± 0.1
RGH-2	134 ± 4	17.8 ± 1.1	13.4 ± 0.7	1.3 ± 0.1
RGH-3	141 ± 5	18.1 ± 1.3	13.8 ± 0.8	1.3 ± 0.1

V. CONCLUSION

The flow around a ICE3 train model was experimentally investigated with High-Speed Particle Image Velocimetry (HS-PIV) at the tunnel simulation facility Göttingen (TSG). Three different roughness element designs have been tested for a boundary layer control. Overall four head shape configurations (CLEAN, RGH-1, RGH-2 and RGH-3) are tested, to compare the effect of different roughness elements on the boundary layer development. The HS-PIV measurements provide two-dimensional informations about the flow velocities $\vec{v}_{\text{flow}}$ within an area of $0.271\,\text{m} \times 0.177\,\text{m}$ sidewise of the track. The velocity magnitude v_{flow} as well

as the velocity components $v_{\text{x,flow}}$ and $v_{\text{y,flow}}$ allow a study of the averaged boundary layer along the train model as well as a comparison of the main boundary layer parameters.

A first comparison of the averaged flow velocity magnitude v_{flow} at a distance of $y_{tc} = -0.12\,\text{m}$ to the track center, respectively to the Technical Specifications of Interoperability (TSI), shows an significant effect of the different roughness elements. It is assumed, that the roughness edge at the lowest height, which is also the closest to the light sheet height and measurement position, has a major effect on the boundary layer at the respective height. Differences in the roughness size at the upper model surface have no significant effect on the considered area along the model. For this measurement height, the effect of the upper vortex generators is first observable in the wake flow. These hypotheses are confirmed by the qualitative visualization of the boundary layer along the model and the analysis of the boundary layer parameters δ_{99}, δ_1, δ_2 and H_{12}. For this study, the artificial boundary layer parameters along the head car are not considered. Along the middle and end car, the displacement thickness δ_1 and the momentum thickness δ_2 show an increase for the rough configurations compared to the clean. Furthermore, the larger lowest roughness of RGH-2,3 cause a higher displacement and momentum thickness compared to RGH-1. It is notable, that δ_1 and δ_2 show a similar trend along the middle car. Both parameters reach a maximum near the second inter-car gap and show a small decrease till the rear end. Nevertheless, the similar trend of δ_1 and δ_2 indicates, that the boundary layer of RGH-1,2,3 approaches a behaviour comparable to the CLEAN configuration near the rear end. This is confirmed by the form factor H_{12}, which shows a stabilization of the boundary layer shape along the end car and reaches a similar value of about $H_{12} = 1.3$ for all configurations. It is notable, that H_{12} is close to the form factor of a turbulent flow around a flat pate of $H_{12} = 1.4$. Although the small decrease of δ_1 and δ_2 along the end car, there might be a comparability. It has to be investigated, if the decrease in δ_1 and δ_2 can be associated with ground effects. With these observations it can be assumed, that this method of boundary layer control can be used to increased the flow around the train model, while the boundary layer shape reaches a stable state at a sufficient model length.

Further investigations have to be done, to analyse the effect of the boundary layer control on the near wake and flow structures. With the results of this study, new roughness elements will be designed to control the boundary layer in a way, that the wake flow and maximum induced flow velocities can be compared to full-scale measurements.

REFERENCES

[1] 2008/232/EG, *Entscheidung der Kommission vom 21. Februar 2008 über die technische Spezifikation für die Interoperabilität des Teilsystems 'Fahrzeuge' des transeuropäischen Hochgeschwindigkeitsbahnsystems*, Amtsblatt der Europäischen Union, 2008.

[2] C.J. Baker, A. Quinn, M. Sima, L. Hoefener, R. Licciardello, *Full-scale measurement and analysis of train slipstreams and wakes. Part 1: Ensemble averages*, Proceedings of the Institution of Mechanical Engineers, Part F: Journal of Rail and Rapid Transit, Vol 228, Issue 5, pp. 451 – 467, 2014 doi:10.1177/0954409713485944.

[3] T.W. Muld, *Slipstream and Flow Structures in the Near Wake of High-Speed Trains*, Royal Institute of Technology Stockholm, 2012.

[4] T.W. Muld, G. Efraimsson, D.S. Henningson, *Wake characteristics of high-speed trains with different lengths*, Proceedings of the Institution of Mechanical Engineers, Part F: Journal of Rail and Rapid Transit, Vol 228, Issue 4, pp. 333–342, 2013.

[5] A. Herbst, T. Muld, G. Efraimsson, *Front Shape and Slipstream for Wide Body Trains at Higher Speeds*, KTH Railway Group, Publication 1402, 2012.

[6] A. Buhr, *Experimentelle Untersuchung der instationären Strömungsstrukturen im Nachlauf eines in Wandnähe bewegten stumpfen Körpers*, master thesis, German Aerospace Center (DLR), Göttingen, Germany, 2015.

[7] J. Nikuradse, *Strömungsgesetze in rauhen Rohren*, VDI-Verlag, Berlin, Germany, 1933.

[8] H. Schlichting, *Grenzschicht-Theorie*, 5th edition, Verlag G. Braun, 1965.

[9] M. Raffel, C. Willert, S. Wereley, J. Kompenhans, *Particle Image Velocimetry*, second edition, Springer, 2007.

[10] PivTec, PIVview2C/3C Version 3.0 - User Manual, PivTec GmbH, Stauffenbergring 21, Göttingen, Germany, 2010.

[11] A. Buhr, A. Henning, K. Ehrenfried, *An Experimental Study of Unsteady Flow Structures in the Wake of a Train Model*, in J. Pombo, (Editor), Proceedings of the Third International Conference on Railway Technology: Research, Development and Maintenance, Civil-Comp Press, Stirlingshire, UK, Paper 41, 2016. doi:10.4203/ccp.110.41.

[12] D.W. Weyburne, *New thickness and shape parameters for the boundary layer velocity profile*, in Experimental Thermal and Fluid Science, Vol 54, pp. 22 – 28, 2014 issn:0894-1777.